Micromorphic continuum stress measures calculated from three-dimensional ellipsoidal discrete element simulations on granular media

R.A. Regueiro, B. Zhang, & F. Shahabi
Department of Civil, Environmental, and Architectural Engineering
University of Colorado, Boulder, United States of America

ABSTRACT: The objective of the paper is to demonstrate the calculation of micromorphic continuum stress measures based directly on three-dimensional (3D) ellipsoidal discrete element (DE) simulations over representative volume elements (RVE) within the DE domain representing granular media. We will demonstrate these calculations for two simulations: (1) pile penetration, and (2) cavity expansion. All calculations are assumed to be performed in the current configuration with respect to a large deformation micromorphic continuum mechanics analysis. The micromorphic continuum stresses include the unsymmetric third order couple stress tensor m_{ijk}, symmetric second order micro-stress tensor s_{ij}, and unsymmetric second order Cauchy stress tensor σ_{ij}. The DE continuum stress measure due to Christoffersen et al. (1981) and Rothenburg & Selvadurai (1981), is used as the symmetric "micro-element" stress tensor σ'_{ij} for micromorphic continuum mechanics (Eringen & Suhubi 1964). The balance equations solved are the balance of linear and angular momenta for the DE simulations, whereas the micromorphic continuum stress measures are only used to interpret the DE simulation results, at the moment.

1 INTRODUCTION

To date, homogenized continuum modeling of granular materials has considered primarily traditional continuum mechanics as the overlaying framework (Christoffersen et al. 1981, Rothenburg and Selvadurai 1981, Chang et al. 1992, Borja and Wren 1995, Mühlhaus et al. 2000, Peters 2005, Andrade and Tu 2009) or higher order methods like micropolar continuum mechanics or enhanced continua with strain gradients (Chang and Gao 1995, Walsh and Tordesillas 2004, Pasternak and Muhlhaus 2005, Gardiner and Tordesillas 2006). These methods involve attempts to either replace the underlying discrete particle mechanics with an equivalent continuum constitutive model, or provide a continuum framework to which to up-scale the discrete particle mechanics through underlying Discrete Element Method (DEM) simulations (Cundall & Strack 1979) via hierarchical up-scaling procedures. We are interested in both approaches, but follow here the spirit of the latter class of methods (hierarchical up-scaling), and we use micromorphic continuum mechanics as the overlaying continuum mechanics framework. In the paper, we focus only on the micromorphic continuum stress measures, and consider micromorphic deformation and strain measures for future work. We focus on the micromorphic theory because of the additional kinematics it provides, through not only the micro-rotation of a micro-element volume (e.g., the Representative Volume Element (RVE) of a granular material), but also micro-stretch and micro-shear. The micropolar theories were primarily motivated for granular materials because of the additional rotational degrees of freedom of the individual particles, but these theories miss the ability to model clusters of particles that also shear and compact/dilate.

1.1 *Brief background on the kinematics of a micromorphic continuum at finite strain*

Figure 1 presents the mapping from the reference configuration $\mathcal{B}_0$ to the current configuration $\mathcal{B}$ through the deformation gradient F_{kK} ($dx_k = F_{kK}dX_K$) and micro-deformation tensor χ_{kK} ($\xi_k = \chi_{kK}\Xi_K$). Ξ_K is the relative position vector between the centroid C of the macro-element differential volume dV and the centroid C' of the micro-element differential volume dV' in the reference configuration $\mathcal{B}_0$. Similarly, ξ_k is the relative position vector between the centroid c of the macro-element differential volume dv and the centroid c' of the micro-element differential volume

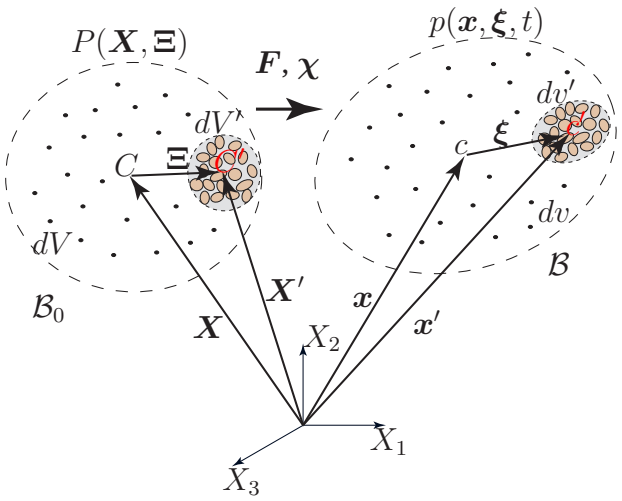

Figure 1: Kinematics of a micromorphic continuum at finite strain.

dv' in the current configuration $\mathcal{B}$. Position vectors of these centroids are indicated in Fig.1. From these basic kinematics, new micromorphic balance equations (including the balance of first moment of momentum, which we use below) can be derived (Eringen & Suhubi 1964, Eringen 1999, Regueiro 2011).

1.2 *Motivation in the context of overlap coupling methods*

Ongoing work involves direct overlap coupling between large deformation micromorphic continuum finite elements (FEs) with underlying DE particles for a concurrent multiscale computational modeling approach for simulating large deformation analysis of granular materials in regions of interest, such as the interface with a tire, penetrometer, or buried explosive simulation (see Fig.2). The purpose of this multiscale framework is to capture as much of the underlying DE particle kinematics and kinetics within the micromorphic continuum FE formulation, such that the DE region can be minimized for computational efficiency, and also to minimize or negate any artificial boundary effects due to the overlap coupling of DE with micromorphic FE close to the interfacial mechanics region (e.g., tire tread, penetrometer surface, etc).

2 HIERARCHICAL UP-SCALING FOR MICROMORPHIC CONTINUUM STRESS CALCULATIONS FROM 3D DEM SIMULATIONS

To start, we recall the symmetric part of the granular stress definition (we call this stress, in the context of a micromorphic continuum, the "micro-element" stress (Eringen & Suhubi 1964)) as (Christoffersen et al. 1981, Rothenburg and Selvadurai 1981)

$$\sigma'_{kl} = \frac{1}{2v^{RVE}} \sum_{\epsilon=1}^{M} (f_k^\epsilon b_l^\epsilon + b_l^\epsilon f_k^\epsilon) \tag{1}$$

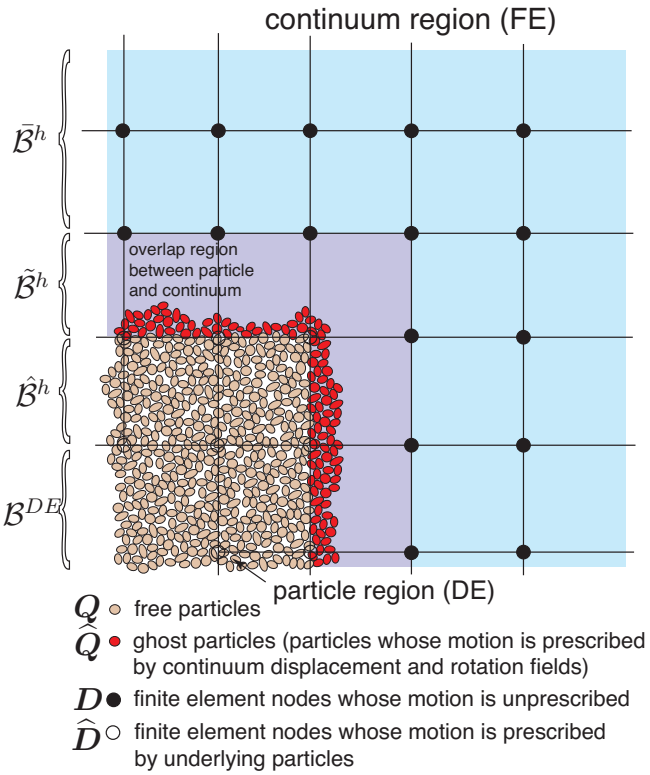

Figure 2: Two-dimensional illustration of the coupling between particle and continuum regions. The purple background denotes the FE overlap region $\tilde{\mathcal{B}}^h$ with underlying ghost particles, aqua blue the FE continuum region $\bar{\mathcal{B}}^h$ with no underlying particles, and white background (with brown particles) the free particle region $\hat{\mathcal{B}}^h \cup \mathcal{B}^{DE}$.

where f_k^ϵ is the interparticle force at contact ϵ, and b_l^ϵ is the branch vector connecting the two particle centroids with contact ϵ. We assume there are M total number of contacts within the RVE volume v^{RVE} at the instant in time when the micro-element stress σ'_{kl} is calculated. These RVE domains (with surface area a^{RVE} and unit normals $\boldsymbol{n}^{RVE}$) comprise an averaging domain $\Omega_\alpha^{\text{avg}}$ with surface $\Gamma_\alpha^{\text{avg}}$ (see Fig.3). The center of $\Omega_\alpha^{\text{avg}}$ is denoted by point c_α, and the center of the RVEs by points c'. The relative position vector ξ_m extends from c_α to c' in the current configuration of the body $\mathcal{B}$ (see Figs.1,3). Essentially, we substitute discrete averaging domain $\Omega_\alpha^{\text{avg}}$ for macroscopic differential volume dv, and discrete RVE domain v^{RVE} for micro-element differential volume dv'. It is assumed that the macroscopic micromorphic continuum measures are calculated at point c_α over discrete averaging domain $\Omega_\alpha^{\text{avg}}$, for $\alpha = 1 \ldots n_{\text{avg}}$, where n_{avg} is the number of averaging domains over the discrete continuum body $\mathcal{B}^h$ in the current configuration, where h is a discretization parameter representing a finite element (FE), finite difference (FD), or meshfree approximation to solve the micromorphic continuum governing equations. The advantage of this approach is to utilize an already well-established micromorphic continuum theory at finite strain (Eringen & Suhubi 1964, Suhubi & Eringen 1964, Eringen 1999), and to focus on an apparent criticism of the theory which is how to determine parameters for the higher order constitutive models (Forest & Sievert 2003, Regueiro 2009,

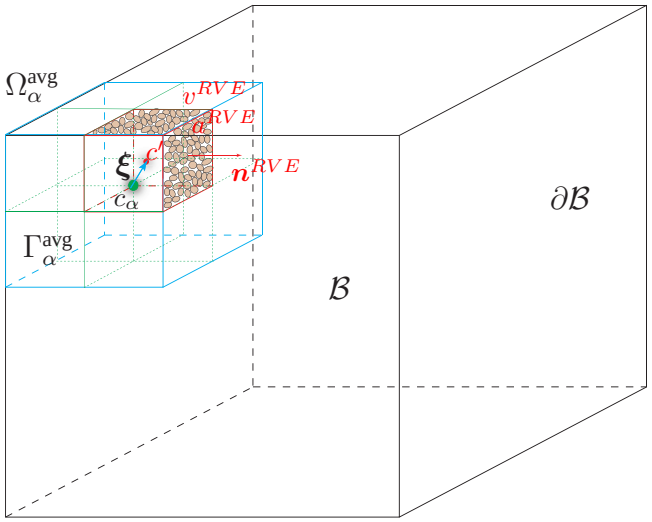

Figure 3: Illustration of averaging domain $\Omega_\alpha^{\text{avg}}$ for micromorphic stress calculation, and smaller RVE volume v^{RVE} for symmetric 'micro-element' granular stress calculation $\boldsymbol{\sigma}'$.

Regueiro 2010).

To continue in this direction, we define, based on the previous discussion, a volume average for the symmetric micro-stress s_{kl} and unsymmetric couple stress m_{klm} as

$$s_{kl} \overset{\text{def}}{=} \frac{1}{\Omega_\alpha^{\text{avg}}} \int_{\Omega_\alpha^{\text{avg}}} \sigma'_{kl} dv' \tag{2}$$

$$m_{klm} \overset{\text{def}}{=} \frac{1}{\Omega_\alpha^{\text{avg}}} \int_{\Omega_\alpha^{\text{avg}}} \sigma'_{kl} \xi_m dv' \tag{3}$$

Before moving on, recall that balance equations are derived by localizing an integral over the body $\mathcal{B}$ in the current configuration. We consider discrete approximations to these integrals (e.g., an eventual Gaussian quadrature rule), such that

$$\int_{\mathcal{B}} (\bullet) dv = \sum_{\alpha=1}^{n_{\text{avg}}} \int_{\Omega_\alpha^{\text{avg}}} (\bullet)' dv' \approx \sum_{\alpha=1}^{n_{\text{avg}}} (\bullet)_\alpha W^{\text{avg}} \Omega_\alpha^{\text{avg}}$$

$$\int_{\Omega_\alpha^{\text{avg}}} (\bullet)' dv' \approx \sum_{RVE} (\bullet)' W^{RVE} v^{RVE} \tag{4}$$

where W^{avg} and W^{RVE} are the weights of integration, which for now we assume $W^{\text{avg}} = W^{RVE} = 1$ (later, these will take appropriate values in the context of a FE, FD, or meshfree numerical implementation). For example, the micromorphic continuum symmetric micro-stress $\boldsymbol{s}_\alpha$ at point c_α within averaging domain $\Omega_\alpha^{\text{avg}}$ can be calculated as,

$$(s_{kl})_\alpha = \frac{1}{\Omega_\alpha^{\text{avg}}} \sum_{RVE} \sigma'_{kl} v^{RVE} \tag{5}$$

and likewise for the micromorphic continuum unsymmetric couple stress $\boldsymbol{m}_\alpha$ as

$$(m_{klm})_\alpha = \frac{1}{\Omega_\alpha^{\text{avg}}} \sum_{RVE} \sigma'_{kl} \xi_m v^{RVE} \tag{6}$$

The question then becomes how to calculate the micromorphic continuum unsymmetric Cauchy stress $\boldsymbol{\sigma}_\alpha$ at point c_α. Recall from the micromorphic continuum theory (Eringen & Suhubi 1964) that the stresses are defined as follows,

$$s_{mk} dv \overset{\text{def}}{=} \int_{dv} \sigma'_{mk} dv' \tag{7}$$

$$\sigma_{kl} n_l da \overset{\text{def}}{=} \int_{da} \sigma'_{lk} n'_l da' \tag{8}$$

$$m_{lkm} n_l da \overset{\text{def}}{=} \int_{da} \sigma'_{lk} \xi_m n'_l da' \tag{9}$$

Thus, the volume average definition for $\boldsymbol{s}$ in (2) and (5) is in line with micromorphic continuum theory in (7), whereas the volume average definition for $\boldsymbol{m}$ in (3) and (6) is an assumption when compared to (9). The unsymmetric Cauchy stress $\boldsymbol{\sigma}$, however, cannot be uniquely determined from (8), nor can it be estimated by a volume average of $\boldsymbol{\sigma}'$ because this is the definition for $\boldsymbol{s}$. Thus, we resort to the balance of first moment of momentum to calculate $\boldsymbol{\sigma}$.

The balance of first moment of momentum of the micromorphic theory, integrated over the body $\mathcal{B}$ in the current configuration, is written as (Eringen & Suhubi 1964, Eringen 1999),

$$\int_{\mathcal{B}} \left[\sigma_{mk} - s_{mk} + m_{lkm,l} + \rho(\ell_{km} - \omega_{km})\right] dv = 0 \tag{10}$$

where ρ is the mass density, ℓ_{km} the body force couple per unit mass, and ω_{km} is the micro-spin inertia. We can analyze each term separately, with in mind that we want to solve for $\boldsymbol{\sigma}_\alpha$ at point c_α:

$$\int_{\mathcal{B}} \sigma_{mk} dv \approx \sum_{\alpha=1}^{n_{\text{avg}}} (\sigma_{mk})_\alpha \Omega_\alpha^{\text{avg}} \tag{11}$$

$$\int_{\mathcal{B}} s_{mk} dv \approx \sum_{\alpha=1}^{n_{\text{avg}}} (s_{mk})_\alpha \Omega_\alpha^{\text{avg}} = \sum_{\alpha=1}^{n_{\text{avg}}} \sum_{RVE} \sigma'_{kl} v^{RVE}$$

$$\int_{\mathcal{B}} m_{lkm,l} dv = \int_{\partial\mathcal{B}} m_{lkm} n_l da \approx \sum_{\alpha=1}^{n_{\text{avg}}} \sum_{RVE} \sigma'_{lk} \xi_m n_l^{RVE} a^{RVE}$$

$$\int_{\mathcal{B}} \rho \ell_{km} dv \approx \sum_{\alpha=1}^{n_{\text{avg}}} \sum_{RVE} \rho' g_k \xi_m v^{RVE}$$

$$\int_{\mathcal{B}} \rho \omega_{km} dv \approx \sum_{\alpha=1}^{n_{\text{avg}}} \sum_{RVE} \rho' a_k^\xi \xi_m v^{RVE} \tag{12}$$

Table 1: Parameters for quartz sand/gravel. If there is a second number, it is associated with the cavity expansion simulation.

Young's modulus E (Pa)	2.9×10^{10}
Poisson's ratio ν	0.25
specific gravity G_s	2.65
inter-particle coef. of friction μ	0.5
inter-particle contact damping ratio	$5\%, 30\%$
particle radii (m)	$0.001 \sim 0.0025$
viscous damping ratio	$2.0/\Delta t$, 0
time step Δt (sec)	$5.0 \times 10^{-6}, 5.0 \times 10^{-7}$

where g_k is the gravity acceleration vector, ρ' is the mass density of particles in v^{RVE}, and $a_k^{\xi} = \ddot{\xi}_k$ is the acceleration of the relative position vector which is important for dynamics problems, as will be seen for the cavity expansion problem in the Numerical Examples. We calculate a_k^{ξ} based on the motion of the relative position vector ξ_k, which tracks the centroids of the RVEs c' with respect to the centroid of the averaging domain c_α. In this case, the RVEs are assumed to move with the particles, as for the cavity expansion example in Section 3.2. Then, substituting (11)-(12) into (10), we can solve for the micromorphic continuum unsymmetric Cauchy stress $\boldsymbol{\sigma}_\alpha$ at point c_α. Note that as $\boldsymbol{\xi} \to \mathbf{0}$, $\boldsymbol{\sigma}_\alpha = \boldsymbol{s}_\alpha$, and the Cauchy stress is symmetric (i.e., it is the same as the symmetric micro-stress, and vice versa). Thus, for certain continuum mechanics problems of interest to geotechnical and geological engineers, the granular material can be treated as a classical continuum such that the assumption $\boldsymbol{\xi} \to \mathbf{0}$ is valid. For specific problems of interest, however, the discrete nature of the granular material from the perspective of a penetrometer in sand, or tire rolling through gravel, $\boldsymbol{\xi}$ is finite, and thus a generalized continuum theory like micromorphic continuum mechanics may provide additional insight into the mechanics of granular media. At the very least, it will be relevant for overlap coupling procedures, as shown in Fig.2, where the degree of freedom (dof) mismatch between DEM and classical FEM in the overlap region is apparent, and the additional dof in the micromorphic continuum should improve such procedures.

3 NUMERICAL EXAMPLES

We demonstrate the hierarchical up-scaling procedure in Section 2 for calculating the three micromorphic continuum stresses (σ_{ij}, s_{ij}, m_{ijk}) by conducting three-dimensional (3D) ellipsoidal DE simulations for two examples: (1) pile penetration, and (2) cavity expansion. Particle properties are indicated in Table 1.

For comparison purposes in the results, we also consider the unsymmetric granular stress definition

$$\sigma_{kl}^{\Omega} = \frac{1}{\Omega_\alpha^{\text{avg}}} \sum_{\epsilon=1}^{N} (b_l^\epsilon f_k^\epsilon) \tag{13}$$

where N is the total number of contacts in $\Omega_\alpha^{\text{avg}}$.

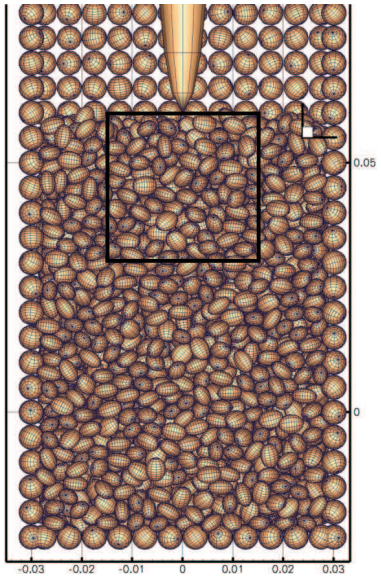

Figure 4: Side view of pile penetration simulation, showing averaging domain $\Omega_\alpha^{\text{avg}}$ drawn by box in the initial penetration zone.

3.1 *Pile penetration*

This example is run quasi-statically, with the 'pile' represented as a large ellipsoidal particle for now (see Fig.4). Further details are found in Yan et al. (2010). The averaging domain $\Omega_\alpha^{\text{avg}}$ is drawn by a box in the initial penetration zone, and is divided into $2 \times 2 \times 2 = 8$ RVEs. These RVEs are fixed. For comparison purposes, the mean couple stress and deviatoric couple stress are defined as follows,

$$(p_m^{\text{couple}})_\alpha \stackrel{\text{def}}{=} \frac{1}{3}(m_{aam})_\alpha \tag{14}$$

$$\Longrightarrow p_\alpha^{\text{couple}} = \sqrt{\boldsymbol{p}_\alpha^{\text{couple}} \cdot \boldsymbol{p}_\alpha^{\text{couple}}}$$

$$\text{dev}(m_{lkm})_\alpha \stackrel{\text{def}}{=} (m_{lkm})_\alpha - (p_m^{\text{couple}})_\alpha \delta_{lk} \tag{15}$$

$$\Longrightarrow \tau_\alpha^{\text{oct,couple}} = \sqrt{\frac{1}{3}} \sqrt{(\text{dev}\boldsymbol{m}_\alpha) \vdots (\text{dev}\boldsymbol{m}_\alpha)}$$

The plots of mean stress and octahedral shear stress are shown in Fig.5, calculated over the averaging domain $\Omega_\alpha^{\text{avg}}$ as discussed in Section 2. They compare the following six stress results: (i) symmetric micro-stress $\boldsymbol{s}_\alpha$, (ii) unsymmetric Cauchy stress $\boldsymbol{\sigma}_\alpha$, (iii) unsymmetric Cauchy stress $\boldsymbol{\sigma}_\alpha$ without micro-spin inertia $\rho\boldsymbol{\omega}$ term in (10), (iv) unsymmetric Cauchy stress $\boldsymbol{\sigma}_\alpha$ without micro-spin inertia $\rho\boldsymbol{\omega}$ and body force couple $\rho\boldsymbol{\ell}$ terms, (v) unsymmetric couple stress $\boldsymbol{m}_\alpha$, and (vi) unsymmetric granular stress $\boldsymbol{\sigma}^{\Omega}$. It is observed that for each mean stress history in Fig.5, as the pile penetrates through the averaging domain $\Omega_\alpha^{\text{avg}}$ (see box in Fig.4), the mean stress increases in compression (negative), and then begins to decrease as the pile passes through $\Omega_\alpha^{\text{avg}}$ (the depth of $\Omega_\alpha^{\text{avg}}$ is 0.03m). Similarly, for octahedral shear stress in Fig.5, the shear stress increases as the particles in $\Omega_\alpha^{\text{avg}}$ shear with respect to each other during pile penetration. Now let us compare the various stress measures. For both mean and

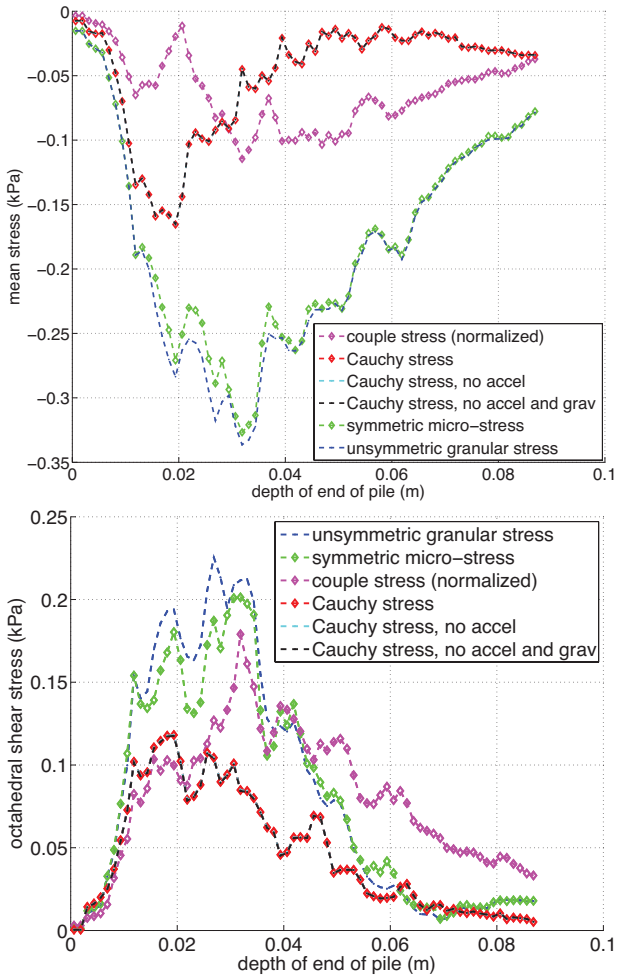

Figure 5: Mean and octahedral shear stress versus time for the various stress measures of the pile penetration example.

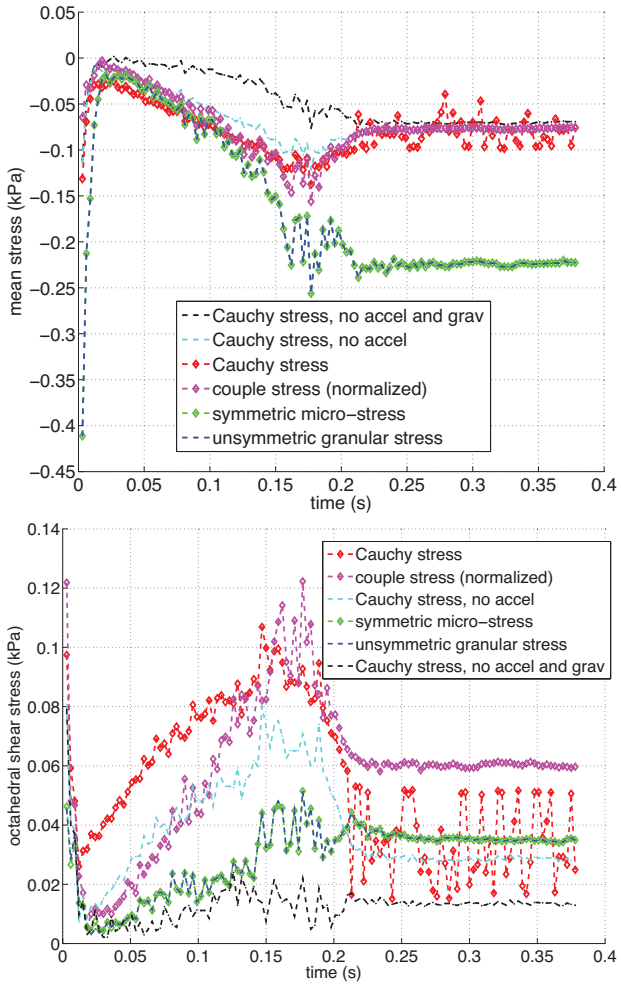

Figure 6: Mean stress and octahedral shear stress versus time for the various stress measures of the cavity expansion example.

octahedral shear stress, the symmetric micro-stress $\boldsymbol{s}_\alpha$ and unsymmetric granular stress $\boldsymbol{\sigma}^\Omega$ are not equal, indicating that the granular stress is unsymmetric. The unsymmetric Cauchy stress $\boldsymbol{\sigma}_\alpha$, as a result of accounting for the couple terms in the balance of first moment of momentum in (10), (11)-(12), shows a reduced value when compared to $\boldsymbol{s}_\alpha$ and $\boldsymbol{\sigma}^\Omega$ in Fig.5, and the effect of acceleration and gravity force couple terms $\rho\boldsymbol{\omega}$ and $\rho\boldsymbol{\ell}$ are negligible. Recall the units of the couple stress, which are Pa.m. Thus, to compare the couple stress values on the same plot, the mean and octahedral shear couple stresses are normalized by the relative position vector $\boldsymbol{\xi}$, which has unit of length; also, $-p_\alpha^{\text{couple}}$ is plotted. Note, the main comparison is between $\boldsymbol{s}_\alpha$ and $\boldsymbol{\sigma}_\alpha$ to see the effect of the length scale (i.e., the relative position vector $\boldsymbol{\xi}$) through the couple stress divergence term in the balance of first moment of momentum. Further work will consider various-sized averaging domains and RVEs to better understand this assumption of length scale (i.e., $\boldsymbol{\xi}$), and its influence on the stresses (and in turn, constitutive equations).

3.2 *Cavity expansion*

This example is run dynamically, where the cavity expansion is started by a high initial outward velocity of an interior cluster of particles, that then pushes the remaining particles (initially at rest under gravity) upward in a box, that then settle down again by gravity (see Fig.7). The changing averaging domain $\Omega_\alpha^{\text{avg}}$ is indicated by the box drawn at various times in Fig.7. This domain is in turn further divided into $4 \times 4 \times 3 = 48$ RVEs. Figure 6 displays the comparison of the stress values over the simulation time for mean and octahedral shear stresses. It is observed that as the cavity expands and pushes the particles up (Fig.7(b)), all mean stress values approach 0 (Fig.6) because there are few particle contacts. As the particles settle by gravity, the mean stress increases in compression (negative), until they come to rest. Similarly for the octahedral shear stress, as the particles reach their maximum height (and least number of contacts) at 0.025s, the octahedral shear stress approaches 0 (Fig.6). Upon settling, the octahedral shear stress increases again, and then decreases to a steady state value when the particles come to rest. Here, the symmetric micro-stress $\boldsymbol{s}_\alpha$ and unsymmetric granular stress $\boldsymbol{\sigma}^\Omega$ are equal, as there is little shearing of particles as compared to the pile penetration problem. For this dynamic example, the significance of the micro-spin inertia $\rho\boldsymbol{\omega}$ and gravity force couple $\rho\boldsymbol{\ell}$ are evident on the calculation of unsymmetric Cauchy stress $\boldsymbol{\sigma}_\alpha$.

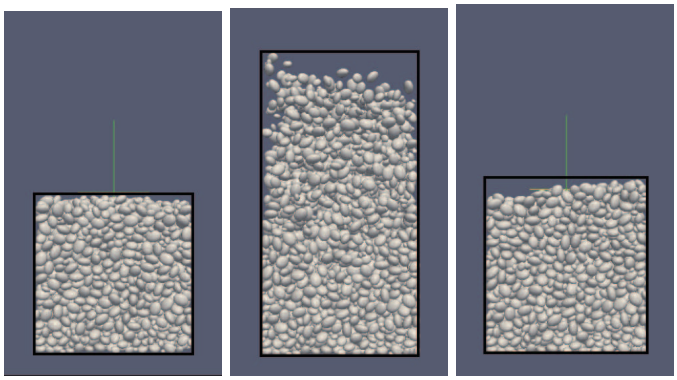

(a) (b) (c)

Figure 7: Side view of cavity expansion simulation, showing averaging domain $\Omega_\alpha^{\text{avg}}$ drawn by box, moving with particles at different simulation times: (a) 0.000s, (b) 0.075s, and (c) 0.375s.

4 CONCLUSIONS

The paper focussed on deriving the equations to calculate the three stresses within a micromorphic continuum theory, for an averaging domain $\Omega_\alpha^{\text{avg}}$ using 3D ellipsoidal DEM simulations: (1) symmetric microstress $\boldsymbol{s}_\alpha$, (2) unsymmetric Cauchy stress $\boldsymbol{\sigma}_\alpha$, and (3) unsymmetric couple stress $\boldsymbol{m}_\alpha$. The stresses $\boldsymbol{s}_\alpha$ and $\boldsymbol{m}_\alpha$ could be calculated directly from volume average definitions, whereas $\boldsymbol{\sigma}_\alpha$ required evaluating the balance of first moment of momentum. Stress results for pile penetration and cavity expansion DEM simulations were compared. It was observed that depending on the example, significant shearing can generate an unsymmetric granular stress $\boldsymbol{\sigma}^\Omega$ as well as Cauchy stress $\boldsymbol{\sigma}_\alpha$ (for pile penetration), and that for dynamics (cavity expansion), the role of micro-spin inertia and gravity couple force can significantly affect the calculation of Cauchy stress $\boldsymbol{\sigma}_\alpha$.

Such a hierarchical multiscale framework for estimating micromorphic stresses, when extended to include the calculation of micromorphic strains, can be used to estimate material parameters of micromorphic constitutive models, as well as which parameters may be set to zero, and also how to estimate the length scale (directly related to the relative position vector $\boldsymbol{\xi}$ in the micromorphic theory). This relies on the DEM model (or other underlying discrete physics-based model) to be physically relevant itself, and there are open questions on that issue that are beyond the scope of the paper (e.g., interparticle constitutive relations, particle shape/fracture, particle mineralogy and crystallographic orientation effects, pore water and air effects, ...).

Future work includes further investigation of the size of the averaging domain $\Omega_\alpha^{\text{avg}}$ and corresponding RVE sizes v^{RVE} within $\Omega_\alpha^{\text{avg}}$, their relative position vectors $\boldsymbol{\xi}$, and resulting stress calculations.

5 ACKNOWLEDGEMENTS

We would like to acknowledge funding for the research from ONR MURI grant N00014-11-1-0691. RAR also acknowledges support from a UPS Foundation visiting professorship in the Department of Civil and Environmental Engineering at Stanford University during the writing of the paper.

REFERENCES

Andrade, J. & X. Tu (2009). Multiscale framework for behavior prediction in granular media. *Mechanics of Materials 41*(6), 652 – 669.

Borja, R. & J. Wren (1995). Micromechanics of granular media. part i: generation of overall constitutive equation for assemblies of circular disks. *Comp. Meth. App. Mech. Engr. 127*(1-4), 13 – 36.

Chang, C., Y. Chang, & M. Kabir (1992). Micromechanics modeling for stress-strain behavior of granular soils. I: Theory. *ASCE J. Geotech. Eng. Div. 118*(12), 1959–1974.

Chang, C. & J. Gao (1995). Second-gradient constitutive theory for granular material with random packing structure. *Int. J. Solids Struct. 32*(16), 2279 – 2293.

Christoffersen, J., M. Mehrabadi, & S. Nemat-Nasser (1981). A micromechanical description of granular material behavior. *J. App. Mech. 48*, 339–344.

Cundall, P. & O. Strack (1979). A discrete numerical model for granular assemblies. *Geotechnique 29*, 47–65.

Eringen, A. (1999). *Microcontinuum Field Theories I: Foundations and Solids*. Springer-Verlag.

Eringen, A. & E. Suhubi (1964). Nonlinear theory of simple micro-elastic solids–i. *Int. J. Engr. Sci. 2*(2), 189 – 203.

Forest, S. & R. Sievert (2003). Elastoviscoplastic constitutive frameworks for generalized continua. *Acta Mech. 160*(1-2), 71 – 111.

Gardiner, B. & A. Tordesillas (2006). Effects of particle size distribution in a three-dimensional micropolar continuum model of granular media. *Powder Technol. 161*(2), 110 – 121.

Mühlhaus, H.-B., L. Moresi, & H. Sakaguchi (2000). Discrete and continuum modelling of granular materials. In D. Kolymbas (Ed.), *Constitutive Modelling of Granular Materials*, pp. 209–224. Springer.

Pasternak, E. & H.-B. Muhlhaus (2005). Generalised homogenisation procedures for granular materials. *Journal of Engineering Mathematics 52*(1), 199 – 229.

Peters, J. (2005). Some fundamental aspects of the continuumization problem in granular media. *J. Eng. Math. 52*(1-3), 231 – 50.

Regueiro, R. (2009). Finite strain micromorphic pressure-sensitive plasticity. *J. Eng. Mech. 135*, 178–191.

Regueiro, R. (2010). On finite strain micromorphic elastoplasticity. *Int. J. Solids Struct. 47*, 786–800.

Regueiro, R. (2011). Nonlinear micromorphic continuum mechanics and finite strain elastoplasticity. ARL-CR-0659, Army Research Laboratory.

Rothenburg, L. & A. Selvadurai (1981). Micromechanical definition of the Cauchy stress tensor for particulate media. In A. Selvadurai (Ed.), *Mechanics of Structured Media*, pp. 469–486. Elsevier Scientific.

Suhubi, E. & A. Eringen (1964). Nonlinear theory of simple micro-elastic solids–ii. *Int. J. Engr. Sci. 2*(2), 389–404.

Walsh, S. & A. Tordesillas (2004). A thermomechanical approach to the development of micropolar constitutive models of granular media. *Acta Mech. 167*(3-4), 145 – 169.

Yan, B., R. Regueiro, & S. Sture (2010). Three dimensional discrete element modeling of granular materials and its coupling with finite element facets. *Eng. Comput. 27*(4), 519–550.